Supplementary information

for

Effects of Substrate Length and Active-Site Residue on Catalytic Function of Fatty Acid Photodecarboxylase

Min-Shih Su[1], *Ya-Ting Kao*[*1,2,3]

[1]Department of Biological Science and Technology, College of Engineering Bioscience, National Yang Ming Chiao Tung University, Hsinchu 30068, Taiwan.

[2]Institute of Bioinformatics and Systems Biology, College of Engineering Bioscience, National Yang Ming Chiao Tung University, Hsinchu 30068, Taiwan.

[3]Center For Intelligent Drug Systems and Smart Bio-devices (IDS[2]B), National Yang Ming Chiao Tung University, Hsinchu 30068, Taiwan.

Supplementary Method
Supplementary Figures: 1-7

Corresponding Author
*** Ya-Ting Kao,** E-mail: yatingkao@nycu.edu.tw

Supplementary Method

Plasmid Design and Protein Expression and Purification

The *Chlorella variabilis* (NC64A) FAP sequence (*cv*FAP Uniprot: A0A248QE08) comprising the FAD-binding domain and the substrate-binding domain (62-654 bp), but excluding the residue transit peptide (TPs, 1-61 bp), was obtained from GenBank (KY511411.1) and further codon-optimized (Figure S1). The codon-optimized *cv*FAP sequence was then subcloned into the *NdeI* and *HindIII* sites of the pET28a vector. *E. coli* BL21 (DE3) pLysS cells containing the plasmid pET28a-*cv*FAP were grown at 37 °C in LB broth containing 50 mg/L kanamycin to an absorption of 0.6 at 600 nm and induced at 17 °C for 18-24 hours with 1 mM isopropyl-β-D-1-thiogalactopyranoside and 400 nM flavin FAD standard. After harvesting, the *cv*FAP protein was purified using the ÄKTA Prime Plus liquid chromatography system with HisTrap HP columns (Ni Sepharose affinity resin). With a gradient elution from 10 to 500 mM imidazole in 50 mM Tris buffer containing 500 mM NaCl and 20% glycerol at pH 8.0, the *cv*FAP was eluted between 150 and 255 mM imidazole. The *cv*FAP was dialyzed in a storage buffer of 50 mM Tris, 500 mM NaCl, and 50% glycerol at pH 8.0. To minimize the photoinactivation effect, samples were kept in the dark throughout the sample preparation processes, including cell culture, sonication, purification, and dialysis.

The SDS-PAGE protein gel for one batch of protein samples from each mutation is shown in Figure S2, with labels indicating the following fractions:

M: Protein marker 1: Crude protein 2: Flow through 3: Washing	4 ~ 14: elute fraction 1 ~ 11

The purity of *cv*FAP, as assessed by SDS–PAGE analysis using an automated gel imaging system (Bio-Rad Gel Doc EZ imager), was approximately 91%, 94%, 92%, and 65% for the wild-type, N170D, N170L, and N170Q variants, respectively. Due to the relatively low expression levels, multiple batches of higher-purity samples were combined for subsequent experiments.

Enzyme-Substrate Binding Assays Analysis

The initial concentration of free *cv*FAP is $[E_T]$ and that of the ligands is $[L_T]$. When reaching the equilibrium of the complex formation, the concentration of the enzyme-substrate or enzyme-product complex (EL) is $[EL]_{eq}$. The dissociation constant K_D of the EL complexes could be represented by

$$K_D = \frac{([E_T] - [EL]_{eq})([L_T] - [EL]_{eq})}{[EL]_{eq}} \quad (1)$$

Thus, $[EL]_{eq}$ could be solved as follows:

$$[EL]_{eq} = \frac{([E_T] + [L_T] + K_D) - \sqrt{([E_T] + [L_T] + K_D)^2 - 4[E_T][L_T]}}{2} \quad (2)$$

Due to quenching effects, the EL complex is weakly fluorescent at 550 nm. If the 550-nm fluorescence of the initial *cv*FAP is F_0 and that of the *cv*FAP-ligand mixture is F_{EL}, the 550-nm fluorescent signal of the mixture is from the free *cv*FAP in the mixture ($[E]_{free} = [E_T] - [EL]_{eq}$). Since the concentration and fluorescence intensity of *cv*FAP were in the linear relationship range, thus,

$$\frac{F_{EL}}{F_0} \propto \frac{[E]_{free}}{[E_T]} = \frac{[E_T] - [EL]_{eq}}{[E_T]} \quad (3)$$

And

$$\Delta F_{550\,nm} = \frac{(F_0 - F_{EL})}{F_0} \propto \frac{[EL]_{eq}}{[E_T]} \quad (4)$$

$$\Delta F_{550\,nm} = A \times \frac{([E_T] + [L_T] + K_D) - \sqrt{([E_T] + [L_T] + K_D)^2 - 4[E_T][L_T]}}{2[E_T]} \quad (5)$$

The analyzed data were plotted with $\Delta F_{550\,nm}$ as Y_{axis} and $[L_T]$ as X_{axis}, and fit by a nonlinear least-squares fitting program with the equation (5), where F_0 is the initial fluorescence intensity in the absence of ligand, F_{EL} is the fluorescence intensity in the presence of ligands of $[L_T]$, E_T is the *cv*FAP initial concentration of 1 μM, L_T is the concentration of the ligand, A is a coefficient related to the fluorescence quantum yield and the extinction coefficient, and the dissociation constant K_D is the unknown parameter that was obtained by fitting our data with equation (5).

L(T) Concentration (μM)	The reaction buffer (Figure 2)	The mild-condition buffer (Figure S4)
Lauric acid (C_{12})	0, 32, 64, 160, 320, 480, 640, 960, 2240.	0, 40, 80, 160, 240, 400, 560, 960, 2240
Palmitic acid (C_{16})	0, 1, 2, 4, 10, 20, 40, 100	0, 1, 2, 4, 10, 20, 30, 80

Arachidic acid (C_{20})	0, 0.2, 0.4, 0.8, 1.6, 2.4, 3.2, 8.0, 20, 40	0, 1, 2, 4, 10, 20, 40, 80, 160

```
   1 GCG AGC GCG GTG GAG GAC ATT CGT AAA GTT CTG AGC GAT AGC AGC AGC CCG GTG GCG GGT
   1 GCG TCT GCC GTT GAA GAC ATC CGT AAA GTC CTG TCC GAT TCT TCG TCT CCG GTG GCG GGT
  61 CAG AAG TAC GAC TAT ATT CTG GTG GGT GGC GGT ACC GCG GCG TGC GTT CTG GCG AAC CGT
  61 CAG AAA TAT GAC TAC ATC CTG GTT GGC GGT GGC ACC GCG GCG TGC GTG CTG GCA AAC CGT
 121 CTG AGC GCG GAT GGC AGC AAA CGT GTG CTG GTT CTG GAG GCG GGT CCG GAC AAC ACC AGC
 121 CTG AGC GCT GAC GGT TCC AAA CGT GTA CTG GTT CTG GAA GCA GGC CCG GAT AAC ACC TCC
 181 CGT GAT GTT AAG ATC CCG GCG GCG ATT ACC CGT CTG TTC CGT AGC CCG CTG GAC TGG AAC
 181 CGC GAC GTT AAG ATT CCG GCG GCG ATC ACC CGC CTG TTC CGC TCC CCG CTG GAC TGG AAC
 241 CTG TTT AGC GAG CTG CAG GAA CAA CTG GCG GAA CGT CAG ATT TAC ATG GCG CGT GGT CGT
 241 CTG TTC TCT GAA CTG CAG GAA CAG CTT GCG GAA CGT CAG ATC TAC ATG GCG CGT GGC CGT
 301 CTG CTG GGC GGT AGC AGC GCG ACC AAC GCG ACC CTG TAC CAC CGT GGC GCG GCG GGT GAC
 301 CTG CTG GGC GGT TCC AGC GCG ACT AAC GCC ACT CTG TAC CAC CGT GGT GCG GCG GGT GAT
 361 TAT GAT GCG TGG GGC GTG GAG GGT TGG AGC AGC GAA GAC GTG CTG AGC TGG TTC GTT CAG
 361 TAC GAC GCA TGG GGT GTT GAA GGC TGG TCC AGC GAA GAC GTT CTG TCT TGG TTC GTC CAG
 421 GCG GAG ACC AAC GCG GAT TTT GGT CCG GGT GCG TAC CAT GGT AGC GGC GGT CCG ATG CGT
 421 GCG GAA ACC AAC GCG GAC TTC GGT CCG GGC GCT TAT CAT GGC AGC GGC GGC CCG ATG CGT
 481 GTG GAA AAC CCG CGT TAT ACC AAC AAG CAA CTG CAC ACC GCG TTC TTT AAA GCG GCG GAG
 481 GTG GAA AAC CCG CGT TAC ACC AAC AAA CAG CTG CAC ACT GCT TTC TTC AAG GCT GCT GAA
 541 GAA GTT GGC CTG ACC CCG AAC AGC GAC TTC AAC GAT TGG AGC CAC GAT CAC GCG GGC TAT
 541 GAA GTT GGT CTT ACC CCG AAC TCC GAT TTC AAC GAT TGG AGC CAT GAC CAC GCC GGT TAC
 601 GGT ACC TTT CAG GTT ATG CAA GAC AAA GGT ACC CGT GCG GAT ATG TAC CGT CAG TAT CTG
 601 GGC ACC TTT CAG GTG ATG CAG GAT AAA GGC ACC CGC GCG GAT ATG TAC CGT CAG TAT CTG
 661 AAG CCG GTG CTG GGC CGT CGT AAC CTG CAA GTT CTG ACC GGT GCG GCG GTG ACC AAG GTT
 661 AAA CCT GTG CTG GGT CGT CGC AAC CTG CAG GTA CTG ACC GGC GCT GCA GTG ACC AAA GTC
 721 AAC ATT GAT CAA GCG GCG GGT AAA GCG CAA GCG CTG GGT GTG GAG TTC AGC ACC GAT GGT
 721 AAC ATC GAC CAG GCT GCG GGC AAA GCG CAG GCT CTG GGT GTT GAA TTC TCC ACC GAC GGC
 781 CCG ACC GGT GAA CGT CTG AGC GCG GAA CTG GCG CCG GGC GGT GAA GTG ATT ATG TGC GCG
 781 CCA ACC GGC GAA CGC CTG TCT GCG GAA CTG GCT CCG GGT GGT GAG GTC ATC ATG TGC GCA
 841 GGT GCG GTT CAC ACC CCG TTC CTG CTG AAA CAT AGC GGC GTT GGT CCG AGC GCG GAG CTG
 841 GGT GCT GTT CAC ACC CCG TTC CTG CTG AAA CAT TCC GGC GTT GGC CCG TCT GCT GAG CTG
 901 AAG GAA TTT GGT ATT CCG GTG GTT AGC AAC CTG GCG GGC GTG GGT CAG AAC CTG CAG GAC
 901 AAA GAA TTC GGC ATC CCG GTT GTT AGC AAC CTG GCT GGT GTT GGC CAG AAC CTG CAG GAT
 961 CAA CCG GCG TGC CTG ACC GCG GCG CCG GTT AAG GAG AAA TAC GAC GGC ATC GCG ATT AGC
 961 CAG CCG GCG TGC CTG ACC GCG GCT CCG GTT AAA GAA AAA TAC GAC GGT ATT GCC ATT TCT
1021 GAT CAC ATC TAT AAC GAA AAG GGT CAA ATT CGT AAA CGT GCG ATT GCG AGC TAC CTG CTG
1021 GAT CAC ATC TAC AAC GAA AAA GGC CAG ATC CGT AAA CGT GCA ATC GCA TCC TAC CTG CTG
1081 GGC GGT CGT GGC GGT CTG ACC AGC ACC GGT TGC GAC CGT GGT GCG TTT GTG CGT ACC GCG
1081 GGT GGT CGT GGC GGT CTG ACT TCC ACC GGT TGC GAT CGC GGT GCC TTC GTT CGT ACC GCG
1141 GGT CAG GCG CTG CCG GAT CTG CAA GTG CGT TTT GTT CCG GGT ATG GCG CTG GAC CCG GAT
1141 GGT CAG GCG CTG CCG GAC CTG CAG GTT CGC TTC GTT CCA GGT ATG GCG CTG GAC CCG GAC
1201 GGT GTG AGC ACC TAT GTT CGT TTC GCG AAG TTT CAG AGC CAA GGC CTG AAA TGG CCG AGC
1201 GGT GTT AGC ACC TAC GTT CGT TTT GCT AAA TTC CAG AGC CAG GGT CTG AAA TGG CCG AGC
1261 GGT ATT ACC ATG CAG CTG ATT GCG TGC CGT CCG CAA AGC ACC GGC AGC GTG GGT CTG AAA
1261 GGC ATC ACC ATG CAG CTG ATC GCT TGC CGT CCG CAG TCT ACC GGC TCC GTC GGT CTT AAA
1321 AGC GCG GAT CCG TTT GCT CCG CCG AAA CTG AGC CCG GGC TAC CTG ACC GAC AAG GAT GGT
1321 TCC GCT GAC CCG TTT GCG CCG CCG AAA CTG TCA CCA GGT TAC CTG ACC GAC AAA GAC GGT
1381 GCG GAT CTG GCG ACC CTG CGT AAA GGC ATT CAC TGG GCG CGT GAT GTT GCG CGT AGC AGC
1381 GCT GAT CTG GCT ACC CTG CGT AAA GGC ATC CAT TGG GCA CGT GAT GTT GCG CGT AGC TCT
1441 GCG CTG AGC GAG TAC CTG GAT GGT GAA CTG TTT CCG GGC AGC GGT GTG GTT AGC GAC GAT
1441 GCT CTG TCC GAA TAC CTG GAT GGT GAG CTG TTC CCA GGT AGC GGC GTT GTT TCT GAT GAT
1501 CAG ATC GAC GAA TAT ATT CGT CGT AGC ATC CAC AGC AGC AAC GCG ATC ACC GGC ACC TGC
1501 CAG ATC GAT GAA TAT ATC CGT CGT TCT ATC CAC TCG TCC AAC GCT ATC ACT GGC ACC TGT
1561 AAG ATG GGC AAC GCG GGT GAC AGC AGC AGC GTG GTT GAT AAC CAG CTG CGT GTG CAC GGC
1561 AAA ATG GGT AAC GCA GGT GAC AGC AGC TCT GTG GTA GAC AAC CAG CTG CGT GTT CAC GGT
1621 GTT GAG GGT CTG CGT GTG GTT GAT GCG AGC GTG GTT CCG AAA ATT CCG GGC GGT CAA ACC
1621 GTT GAA GGC CTG CGC GTT GTT GAC GCT AGC GTT GTT CCG AAA ATT CCG GGT GGT CAG ACC
1681 GGT GCG CCG GTG GTT ATG ATT GCG GAA CGT GCG GCG GCG CTG CTG ACC GGC AAG GCG ACC
1681 GGT GCG CCG GTA GTT ATG ATC GCT GAA CGC GCA GCA GCT CTG CTG ACG GGG AAA GCA ACC
1741 ATC GGT GCG AGC GCG GCG GCG CCG GCG ACC GTT GCG GCG TAA
1741 ATT GGT GCA TCT GCT GCT GCA CCG GCG ACC GTA GCT GCA TAA
```

Figure S1. Comparison of the codon-optimized (*upper*) and native (*lower*, *shaded*) coding sequences of *Chlorella variabilis* GMC oxidoreductases.

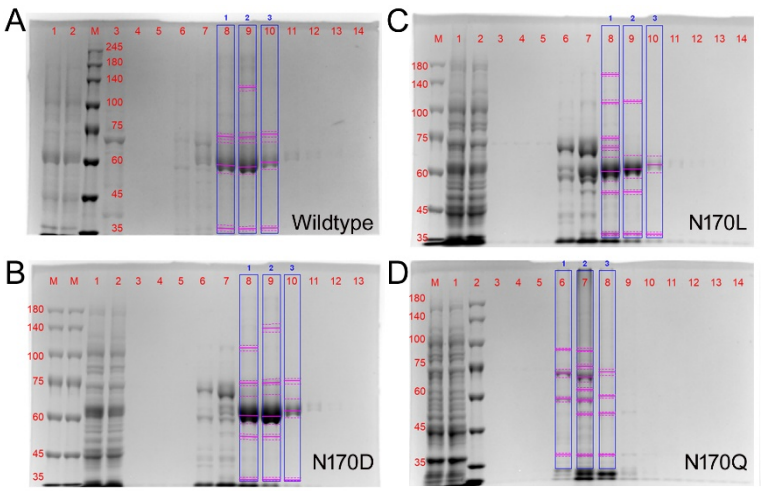

Figure S2. The SDS-PAGE protein gel for one batch of protein samples from each mutation. (A) wildtype *cv*FAP (B) N170D *cv*FAP (C) N170L *cv*FAP (D)N170Q *cv*FAP.

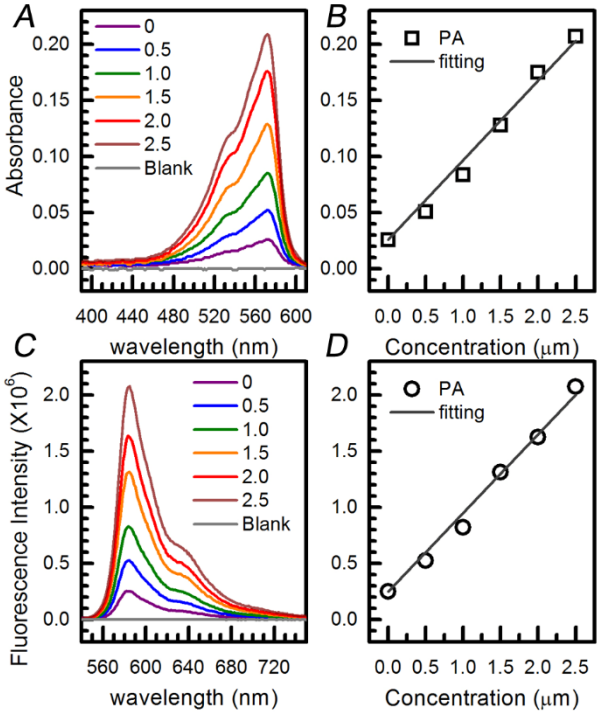

Figure S3. Standard curve for the enzyme activity assay using the ACS-ACOD method. (A) Absorption spectra of the end-products in the ACS-ACOD assay at varying PA concentrations (0 μM to 2.5 μM). (B) A relationship between absorption and PA concentration was used to generate the standard curve for linear regression. (C) Fluorescence spectra of the end-products in the ACS-ACOD assay at varying PA concentrations (0 μM to 2.5 μM). (D) A relationship between fluorescence intensity and PA concentration was used to generate the standard curve for linear regression.

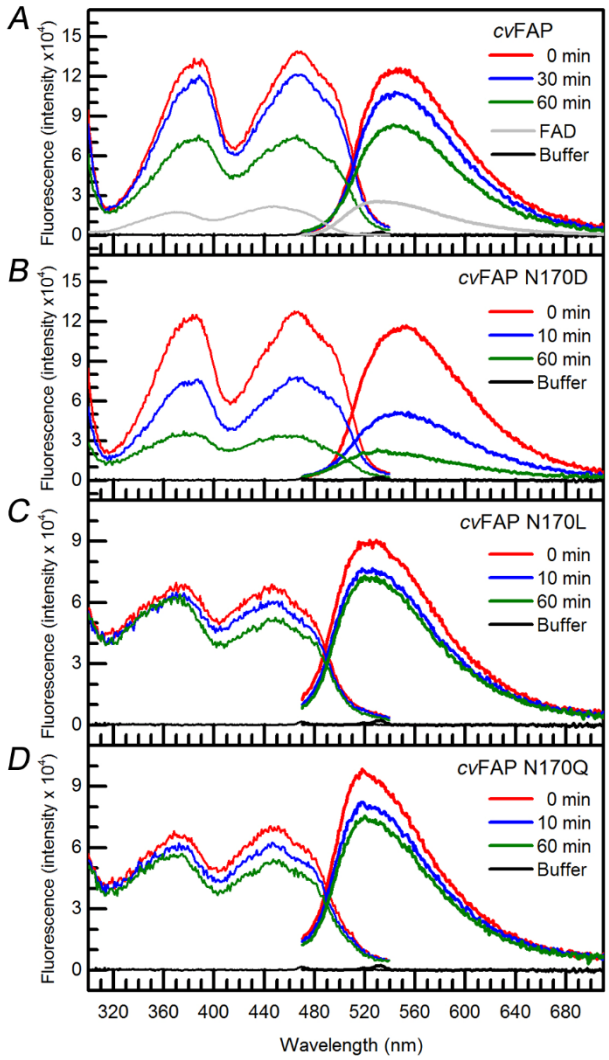

Figure S4. Blue light-dependent inactivation of *cv*FAP and its N170 variants in the reaction buffer. (A) The emission (bold line, 450-nm excitation) and excitation (thin line, 560-nm detection) spectra of *cv*FAP in aqueous solution after 0, 30, and 60 min of 10-mW 450 nm irradiation. The gray trace represents the standard oxidized flavin FAD. (B-D) Emission and excitation spectra of *cv*FAP-N170D, *cv*FAP-N170L, and *cv*FAP-N170Q, after 0, 10, and 60 min of 450 nm irradiation.

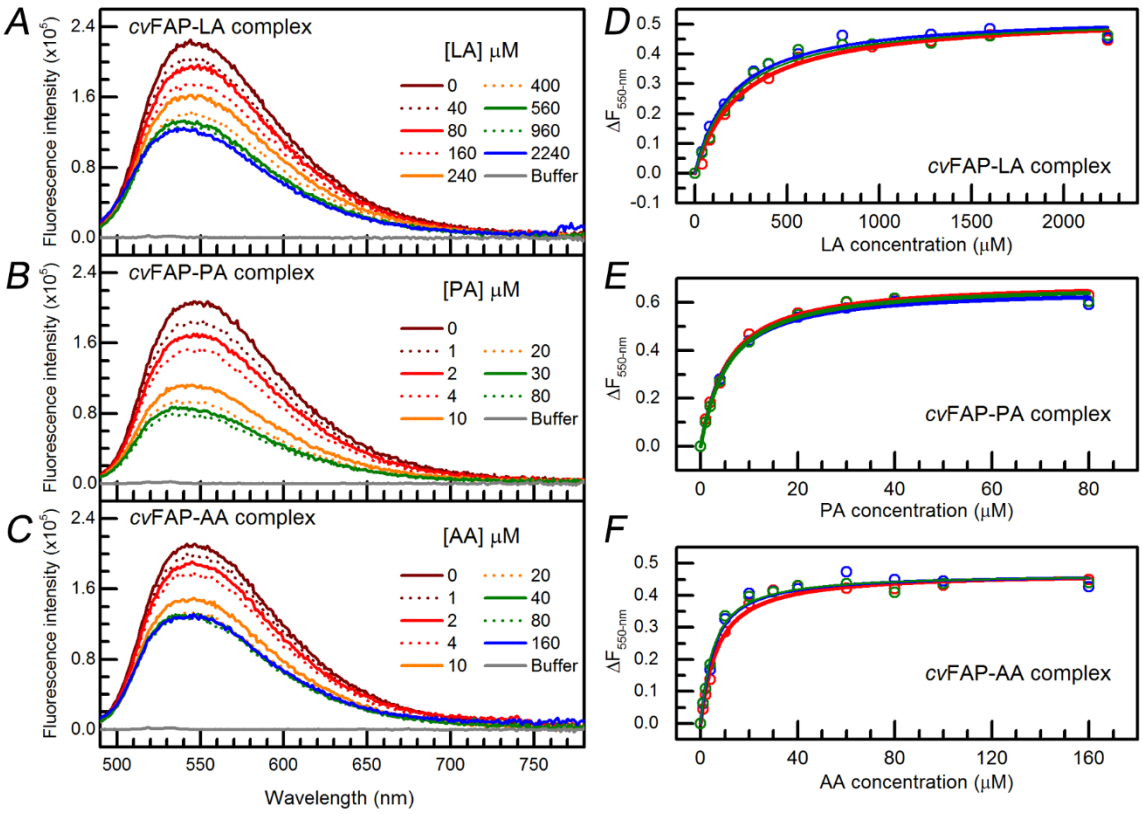

Figure S5. Fluorescence spectra from ligand-binding titration experiments and corresponding analyses in the mild-condition buffer. 1 μM *cv*FAP was titrated with varying ligand concentrations in units of μM. (A) LA-binding titration, (B) PA-binding titration, and (C) AA-binding titration. A decrease in fluorescence at 550 nm was observed as the ligand concentration increased. (D–F) K_D analysis curves. Those detailed analyses are provided in the Supporting Information, and the results are summarized in Table 1.

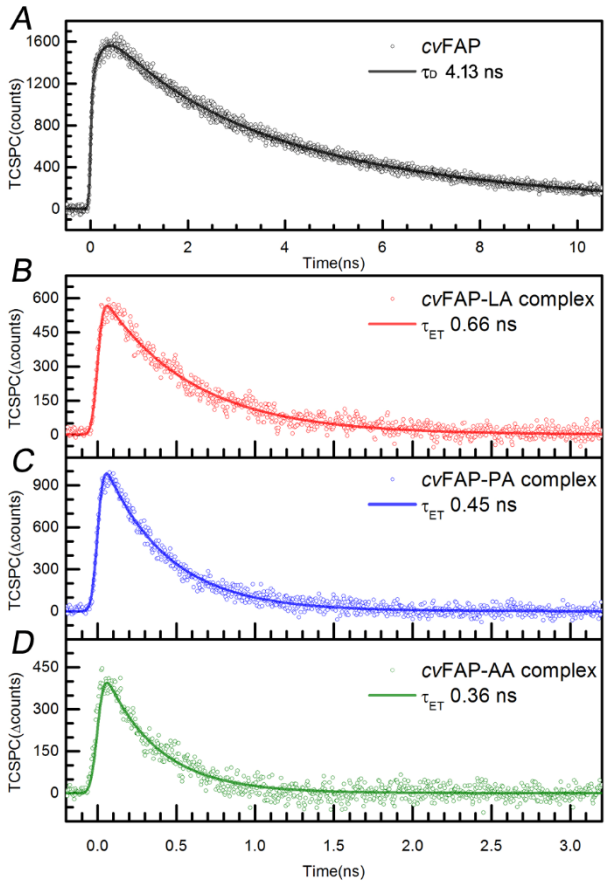

Figure S6. Time-resolved fluorescence decay of *cv*FAP in mild-condition buffer measured by TCSPC. (A) *cv*FAP enzyme and (B–D) various *cv*FAP–substrate complexes. Upon excitation at 450 nm, emission at 560 nm was recorded and analyzed. The fitting model accounts for an additional fast decay component attributed to electron transfer from the substrate to the excited $^{1}FAD^{*}$ cofactor. For clarity, only this fast component is shown.

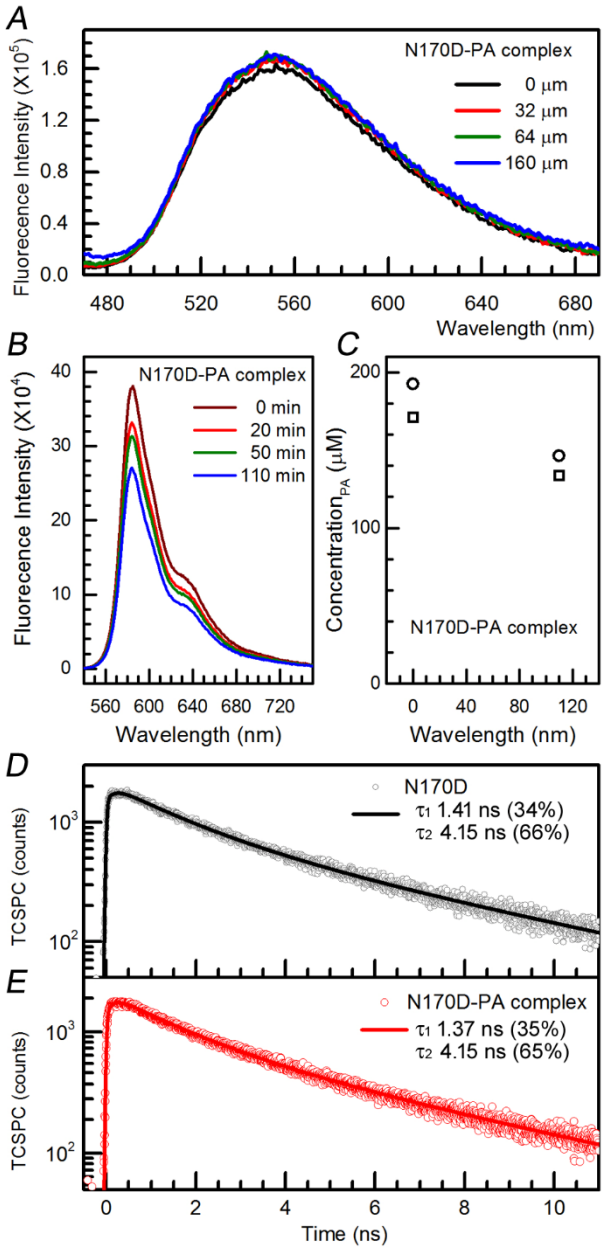

Figure S7. Examination of the N170D variant. (A) Fluorescence spectra from ligand-binding titration experiments conducted in reaction buffer. (B) Enzyme activity assay of the N170D–PA complex in reaction buffer. (C) PA consumption by the N170D–PA complex upon 450 nm irradiation; for clarity, the contribution from other N170 variants has been subtracted. (D, E) Time-resolved fluorescence decay measurements of the N170D variant in the absence and presence of PA substrates, respectively.

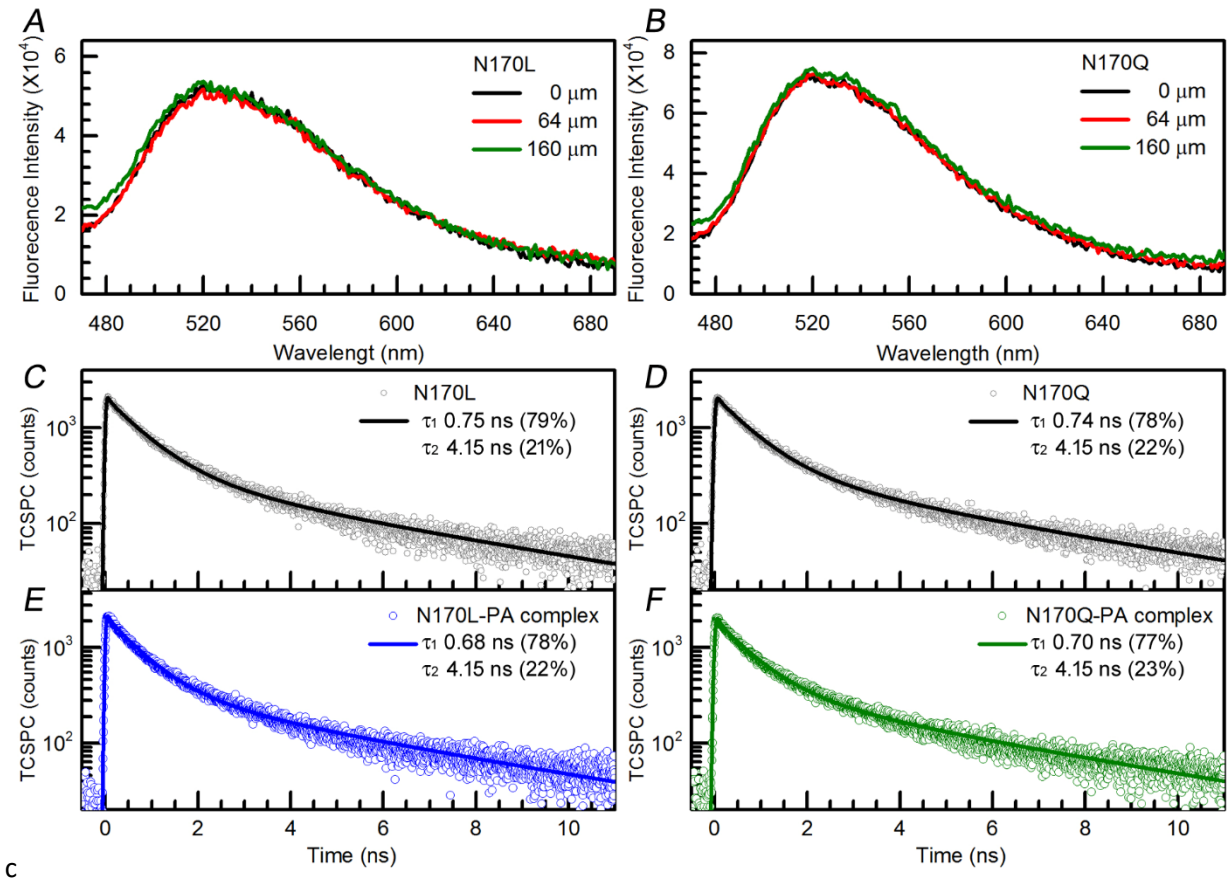

Figure S8. Examination of the N170L and N170Q variants. (A, B) Fluorescence spectra from ligand-binding titration experiments performed in reaction buffer. (C, D) Time-resolved fluorescence decay profiles of the N170L and N170Q variants in the absence of PA. (E, F) Time-resolved fluorescence decay profiles of the N170L and N170Q variants in the presence of PA substrates.